Contact Angle, Wettability and Adhesion, Vol. 2, pp. 1–13
Ed. K.L. Mittal

Effect of electrical potential on adhesion, spreading and detachment of organic droplets at an aqueous electrolyte/metal interface

NADICA IVOŠEVIĆ* and VERA ŽUTIĆ

Ruđer Bošković Institute, Center for Marine and Environmental Research, P.O. Box 180, 10 000 Zagreb, Croatia

Abstract—We demonstrate how spreading and shape of organic droplets at the mercury/aqueous electrolyte interface depend on the interfacial energy that is controlled by the applied potential. We present a method to characterize wetting transients of organic liquids by recording electrical signals of organic microdroplets at the dropping mercury electrode. Electrical signals are fast current transients. The flow of current is caused by double-layer charge displacement due to adhesion and spreading of a single microdroplet. Spike-shaped electrical signals are characterized by the maximum current in μA range, duration in ms time scale and the displaced charge in nC range. This technique thus allows a precise measurement of the area of contact interface assuming validity of the electrical double-layer model. The adhesion of a macroscopic hexadecane droplet at stationary mercury electrode leads to an immediate formation of an underlying monolayer and to a high overpotential (–700 mV) for droplet detachment.

Keywords: Adhesion at mercury electrode; electrical adhesion signals; droplet detachment; dropping mercury electrode; hydrocarbon droplets; wetting transients.

1. INTRODUCTION

The phenomenon of electrowetting [1, 2] and the recent application of an electrical potential to control the shape of organic microdroplets at solid substrates into arrays of lenses, with focal length that can be reversibly changed [3-5], point out to the importance of general understanding of the dynamics and the equilibria of wetting processes at electrodes.

Mercury electrode as a substrate for adhesion studies has several advantages: it is atomically smooth, chemically inert and possesses high surface energy. By varying the electrical potential from 0 to –1.8 V, wetting equilibrium and the dynamics of spreading can be studied in a broad range of interfacial energies over 100 mJ/m^2 [6], Figure 1.

*To whom all correspondence should be addressed. Phone: +385 1 4561-128, Fax: +385 1 4680-242, E-mail: ivosevic@rudjer.irb.hr

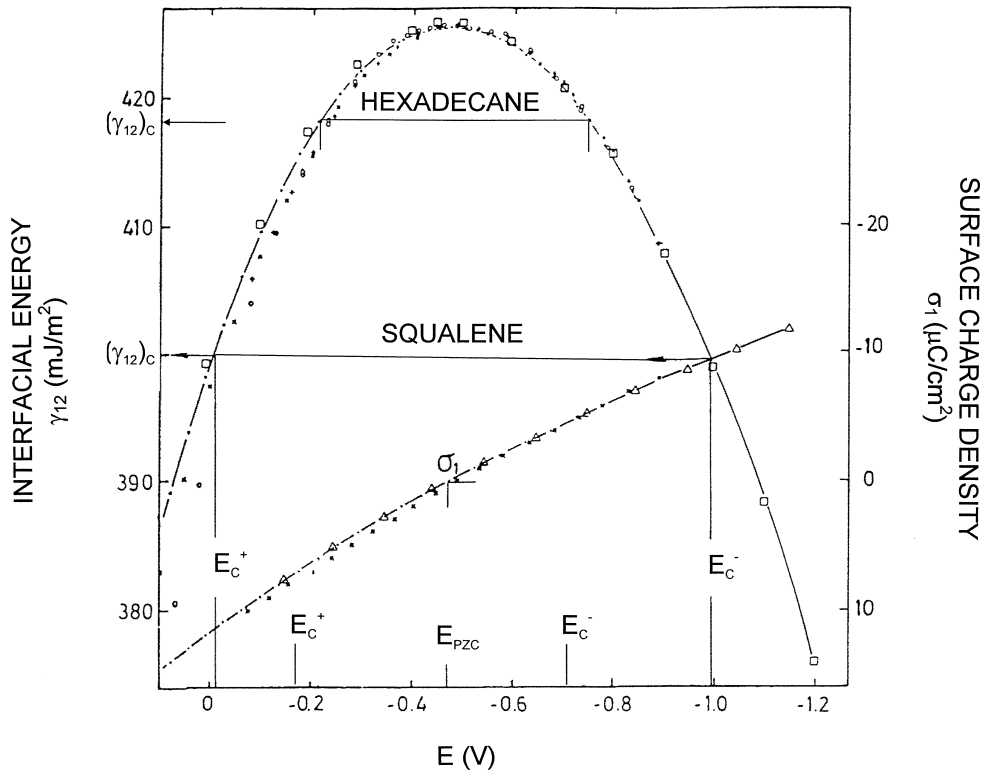

Figure 1. Dependence of interfacial energy (electrocapillary curve) and surface charge density on electrode potential in 0.1 M NaF [18, 19]. The experimental values of the critical potentials of wetting at the positively, E_C^+, and the negatively E_C^- charged interfaces, and the corresponding critical interfacial energies of wetting for the hexadecane and squalene dispersions $(\gamma_{12})_C^+$ and $(\gamma_{12})_C^-$ [9, 10] are indicated on the electrocapillary curve.

The interaction of oil droplets at a mercury/water interface is given by the wetting equilibrium according to the Young-Dupré equation, where the total Gibbs energy of interaction between a droplet and the aqueous mercury interface equals

$$-\Delta G=A\,(\gamma_{12}-\gamma_{23}-\gamma_{13}) \qquad (1)$$

γ_{12},γ_{13} and γ_{23} are the interfacial energies at mercury/water, mercury/oil and water/oil, interfaces, respectively. The expression in parentheses is the spreading coefficient, S_{132}, at the three-phase boundary [7]. When $S_{132}>0$ attachment and spreading are spontaneous processes, while, when $S_{132}<0$, spreading is not spontaneous. The critical interfacial energy of wetting, $(\gamma_{12})_c$ defined by $S_{132}=0$, will be $(\gamma_{12})_c=\gamma_{13}+\gamma_{23}$.

Our previous investigations with dropping mercury electrode, DME, [8-10] immersed in a dispersion of organic droplets in an aqueous electrolyte solution showed that potential controlled interfacial energy determined the wetting equilib-

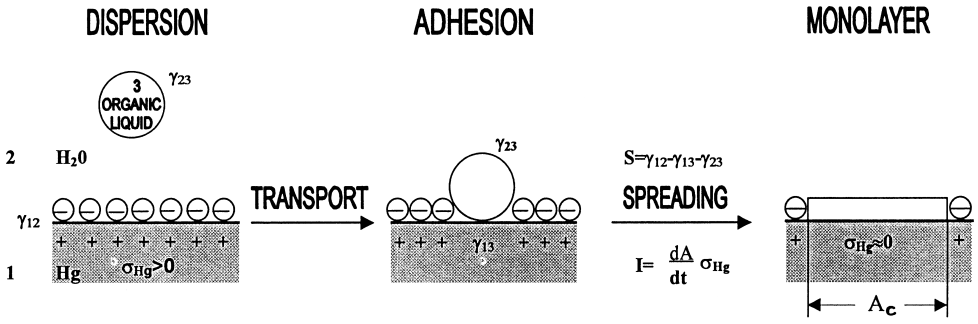

Figure 2. Adhesion of an oil droplet dispersion and its spreading to form a film at the positively charged mercury/aqueous electrolyte interface. Electrical signal is caused by double-layer charge displacement, $((\sigma_{Hg})^{covered}\approx 0)$, from the contact area of the interface (A_c).

rium of droplets and the rate of spreading. Interaction of organic droplets with mercury electrode/aqueous electrolyte interface is presented by a scheme in Figure 2. During the attachment and spreading, organic droplets displace the double-layer charge from the inner Helmholtz plane, and the transient flow of compensating current can be recorded as an electrical signal. Displaced double-layer charge, q_D, can be obtained by integrating the area under the electrical signals

$$q_D=\int I\, dt \tag{2}$$

The extent of spreading could be expressed in terms of the contact interface area, A_c,

$$A_c=q_D/\sigma_{Hg} \tag{3}$$

where σ_{Hg} is the surface charge density of the mercury/aqueous electrolyte interface [8].

Here we compare the effect of electrical potential on adhesion behavior of oil droplets at the stationary and the dynamic mercury/aqueous electrolyte interfaces. Shapes of hexadecane macroscopic droplet at mercury pool electrode/aqueous electrolyte interface were observed visually, while squalene dispersions were used to investigate adhesion signals (displacement current transients) of microdroplets. Hexadecane is the highest n-alkane that is liquid at room temperature with a large number of interfacial data available for calculations of wetting equilibrium [11-14]. Squalene was used due to its wide potential range of wetting (Figure 1) that allows varying the spreading coefficient at the mercury/aqueous electrolyte interface from 0 to 24 mJ/m^2.

2. EXPERIMENTAL

2.1. Experimental setup with mercury pool electrode

A commercial spectrophotometric cuvette was used as the measuring cell with mercury pool working electrode (surface area 6 cm^2), Ag/AgCl reference electrode and Pt wire as a counter electrode forming a three-electrode system [15]. Aqueous electrolyte solution of 0.1 M NaCl was placed above the mercury pool electrode and deoxygenated with a stream of nitrogen. Mercury pool was polarized with a potentiostat. An organic droplet of 70 μL volume was carefully placed directly at mercury/aqueous electrolyte interface at the potential of maximum attraction, –550 mV (Figure 1). Deposition of droplets performed in an open circuit did not lead to attachment.

2.2. Experimental setup with dropping mercury electrode (DME)

The DME had a flow rate of 6.1 mg/s, drop life-time of 2.08 s (at –0.4 V) and a maximum surface area of 4.7 mm^2. All potentials were referred to an Ag/AgCl (0.1 N NaCl) reference electrode separated from the dispersion by a ceramic frit. DME was immersed in an aqueous dispersion of microdroplets in 0.1 M NaF (pH 8.4) in a standard electrochemical cell.

The dispersed phase was squalene (2,6,10,15,19,23-hexamethyl-2,6,10,14,18,22-tetracosahexaene, 99% Sigma). The aqueous dispersion of squalene was prepared by shaking (for 1 hour) 50 μl of squalene in 250 ml of 0.1 M NaF containing 5 mM $NaHCO_3$. All measurements were performed in 25 ml volumes of freshly prepared dispersions and thermostated at 25±1°C. The aliquot of stock dispersion of squalene was added to deoxygenated electrolyte solution prior to measurements. DME was polarized using a PAR 174 Polarographic Analyzer by a linear variation of potential (polarograms) or at constant potentials (amperometric curves). Electrical signals were recorded and stored using a digital oscilloscope connected to a PC computer with a time resolution of 50-200 μs per point. Recording of a series of current-time curves on successive mercury drops was performed since microdroplet arrival and attachment at the electrode is a random process. Droplet size distribution remained virtually unchanged over a period of 20 min, which was sufficient to run the electrochemical experiment.

3. RESULTS AND DISCUSSION

3.1. Hexadecane droplet at mercury pool electrode/aqueous electrolyte interface

The effects of electrical potential on the shape of hexadecane droplet at mercury pool/aqueous electrolyte interface are shown in Figures 3A and 3B. Hexadecane drop (volume 70 μl) forms a planar convex lens at the constant potential of –550 mV (E_{pzc}). The lens changes its shape to semispherical with shifting the potential

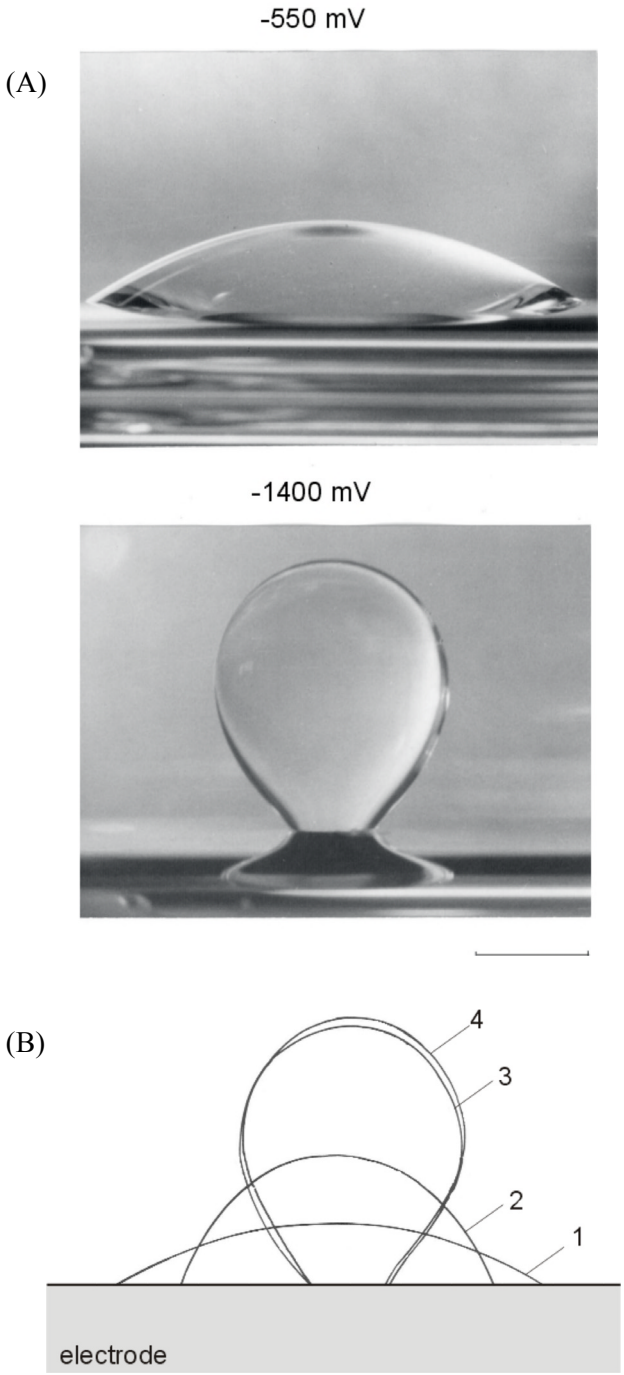

Figure 3. (A) Photographs of n-hexadecane droplet at mercury pool/aqueous electrolyte interface taken at the constant potentials of –550 mV and –1400 mV, bar denotes 2 mm; (B) Contours of droplet shapes at the potentials: –550 mV (1), –1300 mV (2), –1400 mV (3) and –1450 mV (4).

to the more negative values. The droplet remains firmly attached to the mercury interface even at the potentials more negative than the critical potential of wetting, $E_c^- = -730$ mV, Figure 1 [9, 10]. With further changing of potential towards –1400 mV, the droplet changes the shape from semispherical to an ideal sphere, while the contact area decreases. Figure 3B shows contours of droplet shapes at different constant potentials. Only at more negative over-potential, –1456 mV, hexadecane droplet detaches and rises to the surface by buoyancy. At the given potentials, the shapes of hexadecane droplet were established instantaneously. The particular shapes were reproducible in independent experimental series and perfectly repeatable by the successive changes of potential within the range where detachment does not take place. The difference between the potential of the detachment of hexadecane droplet and the critical potential of wetting of $\Delta E = -700$ mV, corresponds to the difference in interfacial energy of 80 mJ/m^2. This difference in interfacial energy [3] can be interpreted by the presence of an underlying hexadecane monolayer, formed immediately upon droplet deposition at the mercury electrode/aqueous electrolyte interface. As little as 0.014% of 70 µl droplet volume would be sufficient to form a monolayer over the entire interface (assuming that the surface area per molecule is 20 Å^2 [16]).

Hence, there is an advantage in employing dropping mercury electrode with its growing and renewable surface and individual microdroplets in study of the adhesion and spreading. In such a system the conditions of simple three-phase wetting equilibria mercury/aqueous electrolyte/organic liquid can easily be achieved ($A_c \ll A_{electrode}$).

3.2. Squalene microdroplets at dropping mercury electrode/aqueous electrolyte interface

Squalene dispersion (180 mg/l) contained 5x10^9 droplets/L in the size-range d= 1-100 µm [8, 17]. 0.1 M NaF was chosen as a supporting electrolyte [18, 19] due to a wider range of working potentials at the positively charged electrode and the absence of specific adsorption of fluoride [9, 10].

Figure 4 shows a typical electrical signal of squalene droplet adhesion appearing at the positively charged electrode interface. The duration of an electrical signal (current transient) is in ms range. The signals are characterized by a steep rising portion followed by a slower decay of the displacement current, implying that the mechanism of oil droplet adhesion should involve fast initial attachment and deformation followed by a slower spreading, forming the contact interface of a finite area (A_c). The signal is followed by a decrease of the baseline charging current due to the lower charge density at film-covered fraction of the interface, $(\sigma_{Hg})^{covered} \ll (\sigma_{Hg})^{free}$. In the vicinity of the critical potential $\Delta E = 80$ mV, $S_{132} \leq 9$ mJ/m^2 and the bell-shape portion of current transient [20] indicates film-reorganization during spreading (a phase transition).

The signals appeared randomly over the time of a mercury drop life due to a random arrival of droplets from the heterodispersion [21]. Maximum current and

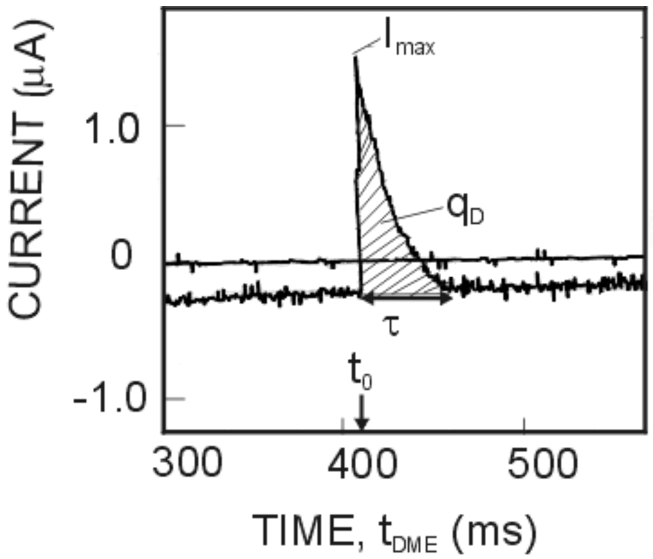

Figure 4. Typical electrical signal recorded in aqueous electrolyte dispersion of squalene microdroplets at the positively charged mercury interface at the potential of –109 mV. The signal is characterized by maximum current (I_{max}), duration of signal (τ) and the time of its appearance (t_0). Shaded area is used to compute displaced charge (q_D).

signal duration depend on droplet size and on spreading coefficient at mercury/aqueous electrolyte interface, which is a function of the applied potential. Assuming that droplet spreading leads to a monolayer formation at the interface (Figure 2) it would be possible to calculate droplet diameter, by knowing the surface area of a squalene molecule in the film [22].

We present here only the signals that appeared at the beginning of a drop life time. Each signal is characterized by the time of its appearance during drop lifetime (t_0), maximum current (I_{max}), duration (τ) and displaced charge (q_D). The electrode interface (A_{DME}) at the time t_0 equals $A_{DME}=0.87\ (6.1x10^{-3})^{2/3}\ t_0^{2/3}$ [23]. Figures 5A and 5B show the signals recorded at the very beginning of drop life at the positively charged electrode, $\sigma_{Hg}=+8.6\ \mu C/cm^2$. The sign of the displacement current is the same as that for reduction and opposite to the charging current of the free mercury surface. The signal 1 in Figure 5A illustrates the adhesion and spreading of a microdroplet at the free electrode surface ($A_c<A_{DME}$), with no detectable decrease in the baseline current after the signal.

The signal 3 in Figure 5B illustrates a more complex case, when $A_c>A_{DME}$. Spreading of the droplet led to a complete coverage of the electrode surface since the baseline charging current after the signal decreased to zero. As the surface area of the mercury electrode continued to grow proportionally to $t^{2/3}$, at the time t_c, the spreading of the droplet proceeded to its maximum extent, i.e. $A_c=A_{DME}$. The analysis of signal 3 gives direct evidence of maximum charge displacement,

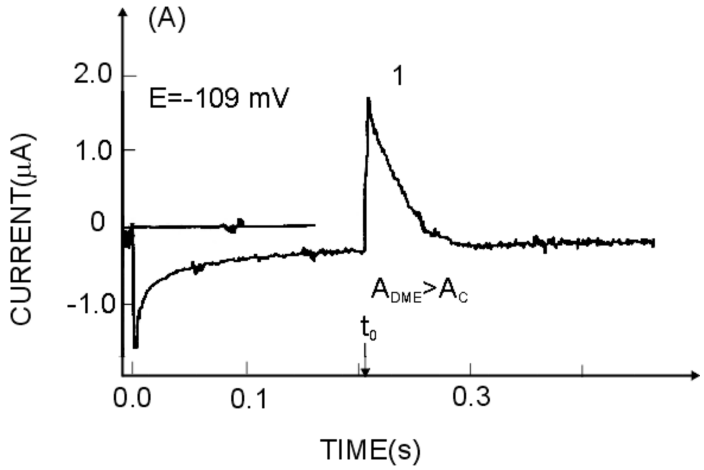

Figure 5A. Segment of current-time curve at the positively charged electrode (E=–109 mV, σ_{Hg}=+8.6 μC/cm^2, γ_{12}=410 mJ/m^2) recorded in the squalene dispersion. Electrical signal 1 appears at the drop life-time t_0, when the electrode surface area exceeds the area of the contact interface, $A_{DME}>A_c$. The number identifies the signal.

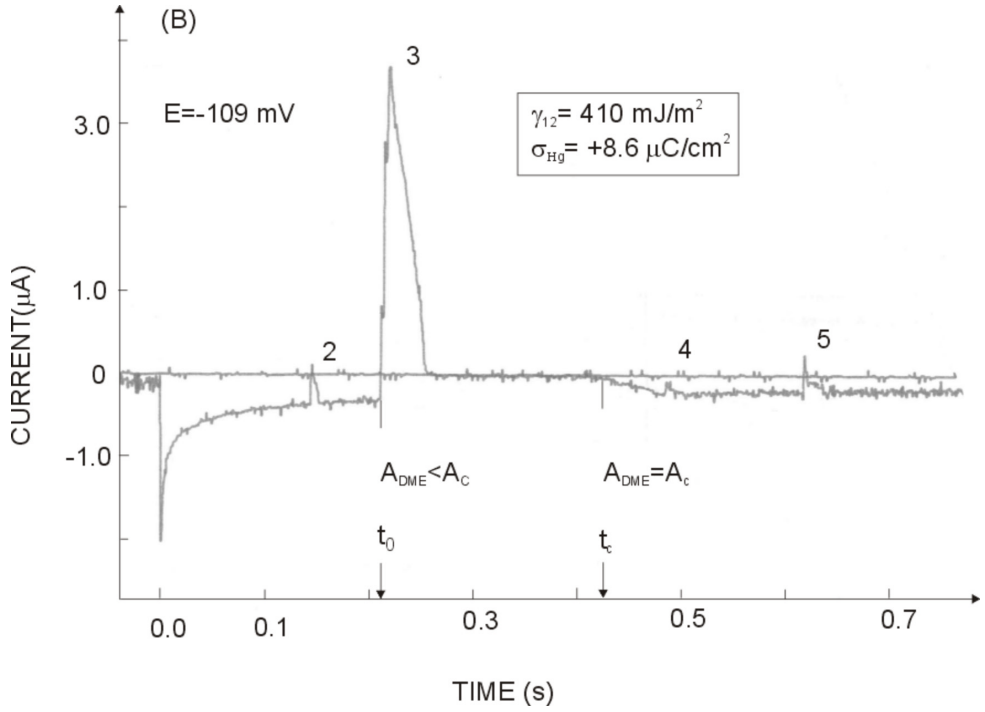

Figure 5B. Consecutive electrical signals 2-5 of squalene droplets recorded at the potential of –109 mV. The signal 3 presents a complex case of total charge displacement: at t_0, $A_{DME}<A_c$; at t_c, $A_{DME}=A_c$; and at $t>t_c$, $A_{DME}>A_c$.

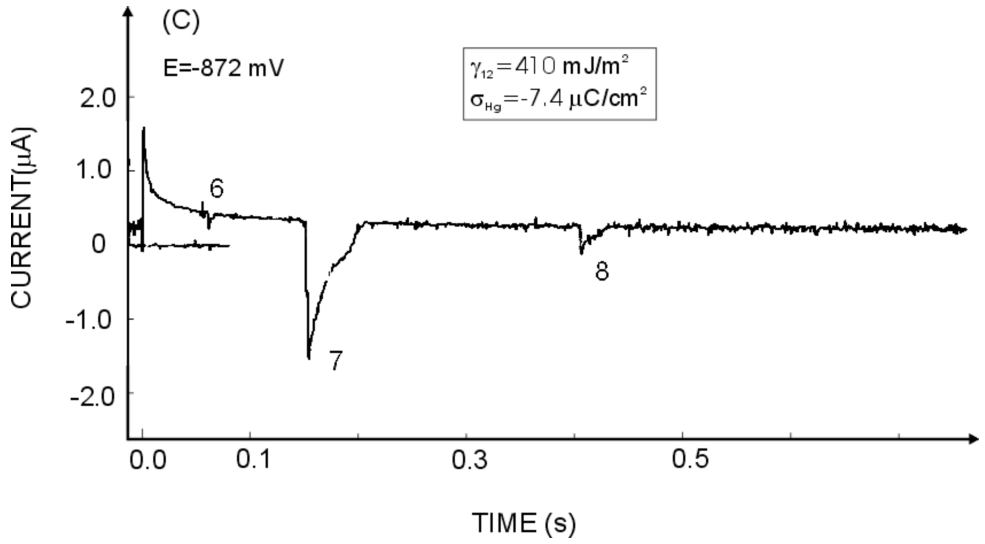

Figure 5C. Consecutive electrical signals 6-8 of squalene droplets recorded at current-time curve at the negatively charged electrode (E=–872 mV, σ_{Hg}=–7.4 μC/cm^2, γ_{12}=410 mJ/m^2).

i.e. $(\sigma_{Hg})^{covered}\approx 0$. The analogous behavior could be identified at the negatively charged interface. Increase of charging current at $t>t_c$ is caused by the appearance of a fresh, free surface area of the electrode. It is important to note that there were no signals at a covered electrode surface, i.e. when I=0. At a partially covered electrode ($t>t_c$), the signals 4 and 5 appeared again but with longer duration than the signal 2, indicating a slower spreading than at the free surface. It is thus possible to follow the dynamics of film spreading over the interface and the dynamics of releasing of free mercury surface in the time spans of $t<t_c$ and $t>t_c$, respectively.

At the potential of –872 mV (Figure 5C) the electrode is negatively charged (σ_{Hg}=–7.5 μC/cm^2) while γ_{12} is equal to 410 mJ/m^2 like that at –109 mV. The electrical signals appear with the opposite direction as mirror images of the signals at –109 mV (Figure 5A). The sign of displacement current is the same as that for oxidation, and opposite to the charging current of the free mercury electrode. This change of the sign of displacement current corresponds to the displacement of double-layer charge from the inner Helmholtz plane and the establishment of direct contact between the squalene droplet and the negatively charged mercury interface. The analysis of the signals shown in Figure 5 is summarized in Table 1.

By changing the applied potential, the interfacial energy (Figure 1) and spreading coefficients change accordingly. Spreading coefficient, S_{132}, defined here as a difference between interfacial energy, $\gamma_{12,}$ and critical interfacial energy of wetting at the mercury/aqueous electrolyte interface, $(\gamma_{12})_c$, is used to express the position of wetting equilibrium at a given potential. Characteristic electrical signals of squalene droplets recorded at γ_{12} of 412 mJ/m^2 and S_{132} of 12 mJ/m^2 at the posi-

Table 1.
Analysis of electrical signals of squalene microdroplets shown in Figures 5 and 6. Each signal is characterized by the time of its appearance during drop life-time (t_0), surface area of mercury electrode at the time t_0 (A_{DME}), maximum current (I_{max}), duration (τ), displaced charge (q_D), area of contact interface (A_c), resulting portion of occupied electrode surface area (A_c/A_{DME}) and equivalent spherical diameter (e.s.d.) of droplets

Signal No	Electrode		Signal properties						
	E (mV)	t_0 (ms)	A_{DME} (mm^2)	I_{max} (μm)	τ (ms)	q_D (nC)	A_c (mm^2)	A_c/A_{DME} %	e.s.d. (μm)
1	–107	204	1.005	1.80	96	59.0	0.680	68.30	10.90
2		144	0.798	0.50	8	2.0	0.023	2.88	3.52
3		212	1.031	3.95	44	91.0	1.060 (1.619)*	>100	>12.62 (14.47)*
4		480	1.767	0.15	20	1.0	0.0001	0.006	0.57
5		616	2.084	0.50	20	2.6	0.030	1.44	3.84
6	–872	64	0.467	–0.20	8	–0.3	0.004	0.87	1.96
7		164	0.870	–1.75	60	–40.0	0.540	62.13	10.08
8		440	1.669	–0.35	28	–2.6	0.035	2.09	4.05
9	–133	132	0.754	6.75	12	26	0.317	42.05	8.43
10	–854	392	1.546	–6.90	20	–0.057	0.760	49.16	11.25

* Values of A_c and e.s.d. were calculated for $A_c=A_{DME}$ at t=420 ms (t_C) in Figure 5B.

tively and the negatively charged interfaces are shown in Figures 6A and 6B, respectively. Compared to the signals at interfacial energy, γ_{12} of 410 mJ/m^2 (Figure 5), the shape of the signals changed to sharp and narrow. The duration of signals was in the range from 4 to 20 ms, depending on the droplet size. By increasing S_{132} to 14 mJ/m^2 (at γ_{12} of 414 mJ/m^2) the duration of the signals was even shorter, $\tau<4$ ms. This behavior of decreasing τ with increasing S_{132} was identified at both the positively and negatively charged interfaces. A detailed analysis of signals is given in Table 1.

The analyses of signals duration, τ, at the positively and the negatively charged electrode were performed for the selected signals with maximum current ($I_{max}\approx3.0$ μA) and appearing during the drop life between 200 and 300 ms. The dependence of $1/\tau$ on spreading coefficient is presented in Figure 7. With increasing the S_{132} towards S_{132}^{max}, $1/\tau$ increased in the same way at the positively and the negatively charged interfaces, showing clearly that the interfacial energy of the mercury electrode was governing the rate of spreading (independently of the polarity of the electrode charge).

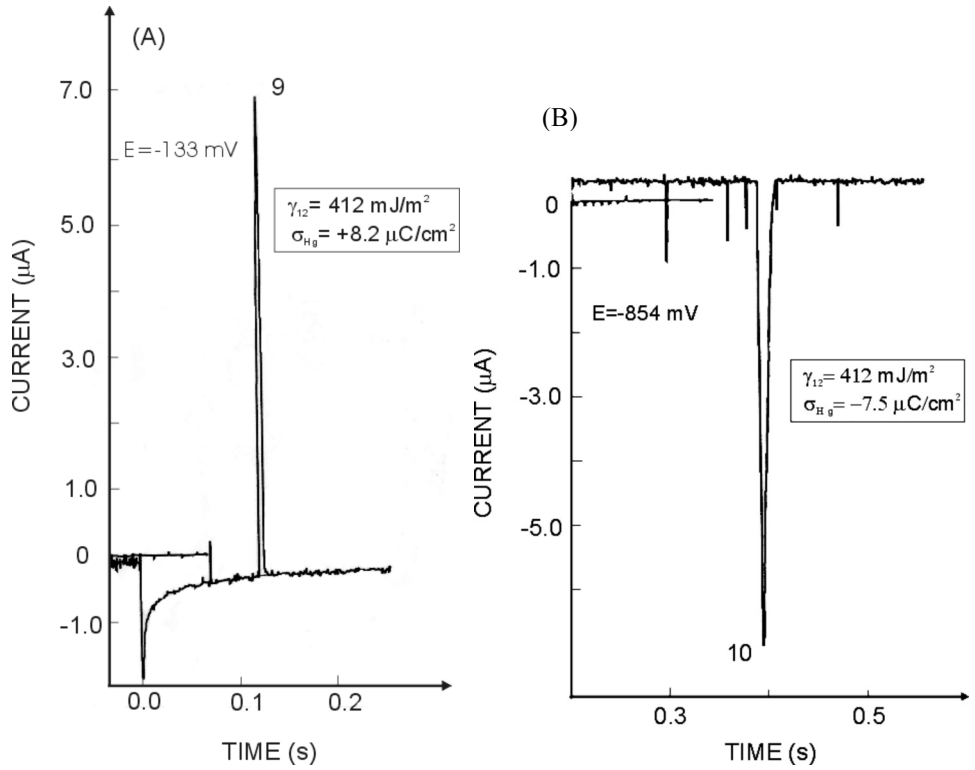

Figure 6. Characteristic electrical signals of squalene microdroplets dispersed in 0.1 M NaF recorded at the potentials: –133 mV (A) and –854 mV (B).

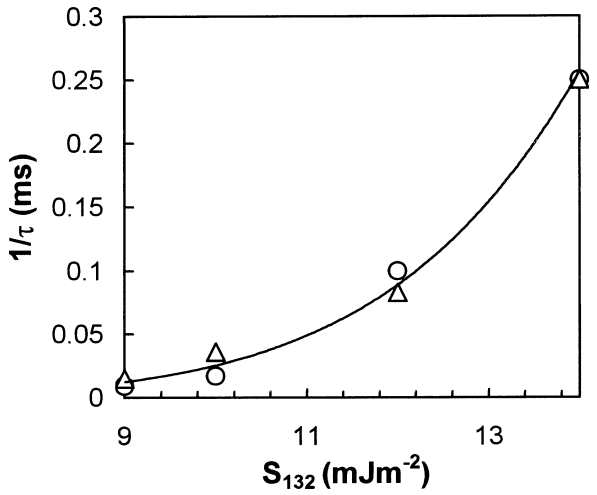

Figure 7. Dependence of signal duration expressed as $1/\tau$, on spreading coefficient at the positively (o) and the negatively (Δ) charged mercury/aqueous electrolyte interfaces.

Potential controlled adhesion of hydrocarbon microdroplets offers a rationale for electrochemical studies of fluid microparticles in aquatic systems [20, 24, 25] and the development of adhesion based sensors for in situ particle analysis [17, 26, 27].

4. CONCLUSION

We have demostrated that the adhesion of organic droplets and the rate of their spreading at the mercury electrode/aqueous electrolyte interface depend on the interfacial energy which is controlled by externally applied electrical potential. Electrical signals of organic microdroplets at a dropping mercury electrode reflect wetting equilibria and the dynamics of spreading at the three-phase system: mercury/aqueous electrolyte/liquid hydrocarbon.

Wetting behaviour of organic liquids could be studied through analysis of displacement current transients of microdroplets at the DME.

Adhesion of macroscopic droplets at a stationary mercury electrode/aqueous electrolyte interface possibly led to the formation of an underlying hexadecane monolayer, requiring a large over-potential for droplet detachment.

Acknowledgements

The research was financially supported by the Ministry of Science and Technology of the Republic of Croatia, Project P-1508.

REFERENCES

1. M. Hato, *J. Colloid Interface Sci.* **130**, 130-136 (1989).
2. H. Matsumoto and J. E. Colgate, *Proc. IEEE Conf. on Micro Electro Mechanical Systems*, Napa Valley, CA, 11-14 February 1990, p. 105.
3. J. A. M. Sondag-Huethorst and L. G. J. Fokkink, *J. Electroanal. Chem.* **367**, 49-57 (1994).
4. C. B Gorman, H. A. Biebuyck and G. M. Whitesides, *Langmuir* **11**, 2242-2246 (1995).
5. W. J. J. Welters and L. G. J. Fokkink, *Langmuir* **14***,* 1535-1538 (1998).
6. J. Lyklema and R. Parsons, *Electrical Properties of Interfaces. Compilation of Data on the Electrical Double Layer on Mercury Electrodes*; Office of Standard Reference Data, National Bureau of Standards, Department of Commerce, Washington DC (1983).
7. J. N. Israelachvili, *Intermolecular and Surface Forces*, Academic Press, New York (1991).
8. V. Žutić, S. Kovač, J. Tomaić and V. Svetličić, *J. Electroanal. Chem.* **349**, 173-186 (1993).
9. N. Ivošević, J. Tomaić and V. Žutić, *Langmuir* **10**, 2415-2418 (1994).
10. N. Ivošević, V. Žutić and J. Tomaić, *Langmuir* **15**, 7063-7068 (1999).
11. F. M. Fowkes, *J. Phys. Chem*. **66***,* 382-383 (1962).
12. F. M. Fowkes, *J. Phys. Chem.* **67***,* 2538-2541 (1963).
13. M. W. Ribarsky and U. Landman, *J. Chem. Phys.* **97**, 1937-1949 *(*1992).
14. R. W. Pastor, *Science* **262**, 223-226 (1993).
15. N. Ivošević and V. Žutić, *Langmuir* **14**, 231-234 (1998).
16. G. Brezesinski, M. Thoma, B. Struth and H. Möhwald, *J. Phys. Chem.* **100**, 3126-3130 (1996).
17. N. Ivošević and V. Žutić, *Croat. Chem. Acta* **70**, 167-178 (1997).

18. N. H. Coung, C. V. D'Alkaine, A. Jenard and H. D. Hurwitz, *J. Electroanal. Chem*. **51**, 377-393 (1974).
19. C. D. Russel, *J. Electroanal. Chem.* **6**, 486-490 (1963).
20. V. Žutić and J. Tomaić, *Marine Chem*. **23**, 51-67 (1988).
21. V. Žutić, V. Svetličić and J. Tomaić, *Pure Appl. Chem*. **62**, 2269-2276 (1990).
22. J. Tomaić, T. Legović and V. Žutić, *J. Electroanal. Chem*. **322**, 79-92 (1992).
23. J. Heyrovský and J. Kuta, *Principles of Polarography*, Chechoslovak Academy of Sciences, Prague (1965).
24. V. Žutić, T. Pleše, J. Tomaić and T. Legović, *Mol. Cryst. Liq. Cryst.* **113**, 131-145 (1984).
25. V. Žutić and T. Legović, *Nature* **328**, 612-614 (1987).
26. F. Baldi, N. Ivošević, A. Minacci, M. Pepi, R. Fani, V. Svetličić and V. Žutić, *Appl. Environ. Microbiol.* **65**, 2041-2048 (1999).
27. V. Svetličić, N. Ivošević, S. Kovač and V. Žutić, *Langmuir* **16**, 8217-8220 (2000).